Geomorphology 183 (2013) 96–109

Contents lists available at SciVerse ScienceDirect

Geomorphology

journal homepage: www.elsevier.com/locate/geomorph

An assessment of the fluvial geomorphology of subcatchments in Parana Valles, Mars

B.G. Nicholson [a], G.R. Hancock [a,*], S. Cohen [b,c], G.R. Willgoose [b], Olivier Rey-Lescure [a]

[a] School of Environmental and Life Sciences, The University of Newcastle, Callaghan, New South Wales, 2308, Australia
[b] School of Engineering and Built Environment, The University of Newcastle, Callaghan, New South Wales, 2308, Australia
[c] Department of Geography, University of Alabama, Box 870322, Tuscaloosa, AL 35487-0322, USA

ARTICLE INFO

Article history:
Accepted 20 July 2012
Available online 27 July 2012

Keywords:
Digital elevation model
Geomorphology
Hydrology
Mars
Erosion
Remote sensing

ABSTRACT

This paper uses a multifaceted remote sensing and morphometric approach to investigate if the surface of subcatchments in the Parana Valles area of Mars (20–30°S, 0–20°W) is reflective of hydrology and sediment transport by water. Using digital elevation model (DEM) data obtained from the Mars Orbiter Laser Altimeter (MOLA), three nested subcatchments were examined using a suite of terrestrial geomorphic and hydrologic statistics to determine if their shape and form lies within the known range of fluvial catchment properties on Earth. Further, an examination of statistical accuracy via an innovative pixel-by-pixel solution of two statistics established that despite mineralogical homogeneity confirmed by the Compact Reconnaissance Imaging Spectrometer for Mars (CRISM) spectral survey, erosion processes were likely to be variable across the study site. The DEM-based methods outlined here can be employed at other sites to investigate geomorphic properties and attributes of the Martian surface.

1. Introduction

Past and contemporary studies of the Martian surface have long theorised the role that water (McCauley et al., 1972) potentially has played in shaping the planetary landscape we see today (Carr, 1981, 1996; Hynek and Phillips, 2001). Images of Mars have provided compelling geomorphic and hydrologic evidence of fluvial-like features on the surface of the planet including valley networks (McCauley et al., 1972; Hynek and Phillips, 2003).

In recent years these data has also been made publicly available to the scientific community via the Planetary Data System (PDS) Geosciences Node of the University of Washington in St Louis (http://geo.pds.nasa.gov/), resulting in an expansion of Mars exploration and discovery.

Valley networks were discovered almost simultaneously with Martian channels (McCauley et al., 1972). Almost all valley network systems on Mars date from the pre-Noachian era (c. 4.6–3.5 Ga) (Fasset and Head, 2008) (however the period 4.56 to ~4.2, the time from which no surface record is available is sometimes called "pre-Noachian") and are overwhelmingly located on the oldest stratigraphic unit visible on the surface, the heavily weathered highlands of the southern hemisphere (Scott and Tanaka, 1986; Carr, 1996). Valley networks are characterised by semi-dendritic patterns that are strikingly similar to terrestrial rivers. Previously, there has been substantial debate concerning whether such networks have been formed by precipitation and surface runoff or headward collapse (sapping) (Pieri, 1980; Squyres and Kasting, 1994; Carr, 1996; Craddock and Howard, 2002).

Erosion of valley networks by precipitation and surface runoff could have occurred in climatically favourable conditions. Evidence of regional erosion and crater degradation from rainfall has also been found in the Margaritifer Sinus and Arabia regions of Mars (Hynek and Phillips, 2003; Howard, 2007). The theory that erosion by runoff occurred stems from observations that valley networks form clear drainage basins and river-like networks or linearments which have been visible since the earliest Mariner 6 images (McCauley et al., 1972).

In contrast, headwall sapping favours a mechanism that does not involve rainfall, but the flow of groundwater as an undermining agent of lower strata, causing collapse at the head of the valley. Amphitheatre terminations in valley networks are commonly used as morphological evidence of a final collapse in channels (Pieri, 1980). Groundwater that is driving this sapping mechanism has been postulated to occur by one of two mechanisms:

1) The groundwater is heated from the Martian core, causing a change in water density gradients at the centre and edge of the plume, initiating flow (Squyres and Kasting, 1994). This is melting of ground ice and water flow by geothermal heating. Further, impact induced heat from meteorites may also produce flows (Solomon et al., 2005).
2) Groundwater is recharged through precipitation at valley heads (Grant, 2000). The rainfall amount and intensity may also have been influenced large impacts which evaporated subsurface ice and injected it into the atmosphere that rained out at decadal time scales.

* Corresponding author.
E-mail address: Greg.Hancock@newcastle.edu.au (G.R. Hancock).

0169-555X/$ – see front matter.
http://dx.doi.org/10.1016/j.geomorph.2012.07.018

How the surface runoff or sapping system is recharged remains a key question in advancing our understanding of Martian climate (Solomon et al., 2005; Barnhart et al., 2009). A clear relationship between drainage area and discharge would justify surface flow theories. However we currently lack the geomorphic data at sufficient resolution from digital elevation models as well as the quantitative discriminatory tools to fully evaluate these processes as geomorphic processes as operating or otherwise.

Previous studies have demonstrated that traditional morphometric statistics such as the hypsometric integral and Strahler statistics are comparable to those on Earth for valley network systems on Mars (Cabrol et al., 2001; Luo, 2002; Ansan and Mangold, 2006). However, this paper is the first investigation of the Martian surface at the sub-basin scale (<7000 km^2) and employs a suite of more recent hydrologic and geomorphic descriptors to compare form and function of catchments in areas where the influence of crater impact on surface morphology is minimal. This approach removes the complexity induced by pit-removal from the DEM from which this study is based.

Examination of geomorphic and hydrologic catchment descriptors derived from digital elevation model data provides quantitative evidence of network organisation, area and slope organisation and erosion processes, and hence an indication of the environment under which the catchments originally formed. These formation conditions are an integral part of determining the geological history of Mars, factors involved in paleoclimate and exobiology models of Mars and simulation of the Martian surface in plans for future exploration. While this paper examines and discusses the fluvial history of Mars, we also focus on methods to assess catchment form and function using well accepted as well as novel techniques for landscape assessment. An interpretation of the results in terms of landscape history is also presented.

2. Study site

The present study examines Martian catchment formation and surface processes using catchment shape and form at Parana Valles, which is located in the Margaritifer Sinus region on Mars (0–30°S, 315–360°E) (USGS quadrangle MC-19SE). The region contains two types of landforms typical of what are believed to be fluvially modified areas on Mars, (1) the Uzboi–Ladon–Margaritifer outflow channel and (2) several smaller-scale valley networks including the Samara and Parana–Loire valley networks. Parana Valles itself is a series of nested and channelised catchments which cluster around the nearby Parana Basin, the largest local depression in the area. These catchments drain into a junction 20 km northeast of Novara Crater (Fig. 1).

This region is a highly researched site on Mars that is believed to have evolved through fluvial erosion (Grant, 1997, 1998, 2000; Grant and Parker, 2002; Luo, 2002). Further, it has a relatively uncratered, pristine surface, requiring little alteration to flow paths in order to drain to an outlet (Fig. 2). It also lies on the oldest stratigraphic units still present on the surface of the planet, the Noachian basement unit (Nb) which encompasses the era of fluvial erosion on the planet during the period from 4.1 to 3.7 billion years ago (4.1–3.7 Ga) (Scott and Tanaka, 1986).

It is noteworthy that Parana Valles is likely to have undergone surface modification from wind, slumping and impact gardening (Hartmann et al., 2001) (impact gardening is the creation and mixing of regolith during surface impact events—see Hartmann et al. (2001) for a more detailed explanation) which could potentially affect geomorphic analysis. Yet, Parana Valles remains one of the better defined channel networks on Mars (Hoke and Hynek, 2009).

3. Method

The primary data set used in this project is altimetry data captured by the MOLA instrument and collated into a regular grid DEM and interpolated to a pixel size of 1/128° per pixel (equal to 463 m per pixel). The version used in this paper (Version L) has an absolute vertical accuracy of 1 m (PDS Geosciences Node).

Here, tiles of the MOLA DEM were visually examined for catchments which had minimal disruption of surface flow due to impact cratering. As the impact craters may cover a significant area of the region and the removal of these depressions causes a major change in both elevation and consequent flow structure it was considered important to select catchments where the need for pit-removal was minimal. However, it was impossible to find catchments which were completely devoid of pits. Extracted catchments with minimal disturbance from crater impact (Figs. 1, 2) were then pit-filled before being analysed statistically by catchment descriptors. The Tarboton et al. (1989) method was used to remove all pits in the data.

Catchment descriptors are useful to planetary geomorphologists as the shape of a catchment and its hydrological organisation can be an indicator of conditions in which the catchment was formed (Cabrol et al., 2001). Catchment area–slope relationships, hypsometric curves and integrals, cumulative area distributions (CAD), width functions and networking properties (Strahler statistics) are presented in results. The above measures are standard methods of catchment assessment on Earth (Hancock, 2005) and this study is the first to apply these on Mars for catchment assessment. In particular, the hypsometric integral has been used widely in other, non catchment-based, Martian work (Luo, 2002; Fortezzo and Grant, 2004; Ansan and Mangold, 2006).

In addition to the above measures a further analysis examining the area–slope relationship and hypsometric integral within the catchment at the pixel scale was undertaken (Cohen et al., 2008). Catchment descriptors are described below.

3.1. Area–slope relationship

The area–slope relationship (Flint, 1974; Tarboton et al., 1989; Willgoose et al., 1991) can be defined as the relationship between the area draining through a point in the catchment and the slope at that point (Willgoose, 1994), and is most often expressed in the form:

$$A^{\alpha}S = \text{constant} \quad (1)$$

where A is the area draining through a defined point in the catchment, S is the slope of that point and α is the scaling exponent. In undisturbed terrestrial fluvial catchments, α ranges between 0.2 and 0.7 (Tarboton et al., 1989; Moglen and Bras, 1995a; Vogt et al., 2003).

Catchment data from Earth demonstrate a break in the scaling exponent α which defines two separate erosion regimes in the catchment (Fig. 3). Left of the breakpoint is the diffusive region, characterised by small contributing areas and high slopes, subjected to diffusive erosion via rainsplash, inter-rill erosion and soil creep which smooth the landscape (Hancock, 2005). To the right of this breakpoint the slope decreases as the area increases, as a result of incisive fluvial erosion in these regions.

3.2. The hypsometric curve and integral

The hypsometric curve compares the normalised elevation versus normalised area of a catchment (Langbein, 1947). The curve is dimensionless, due to the normalisation process of the calculation, and allows catchments of different sizes and elevations to be compared (Willgoose and Hancock, 1998; Hancock, 2005). Strahler (1964) used the curve as an indicator for geomorphic maturity of catchments (Fig. 4) and it has since been demonstrated by Willgoose and Hancock (1998) that different curvature in the head, body and toe of a curve correspond to differing catchment forms, network properties and erosion regimes on Earth.

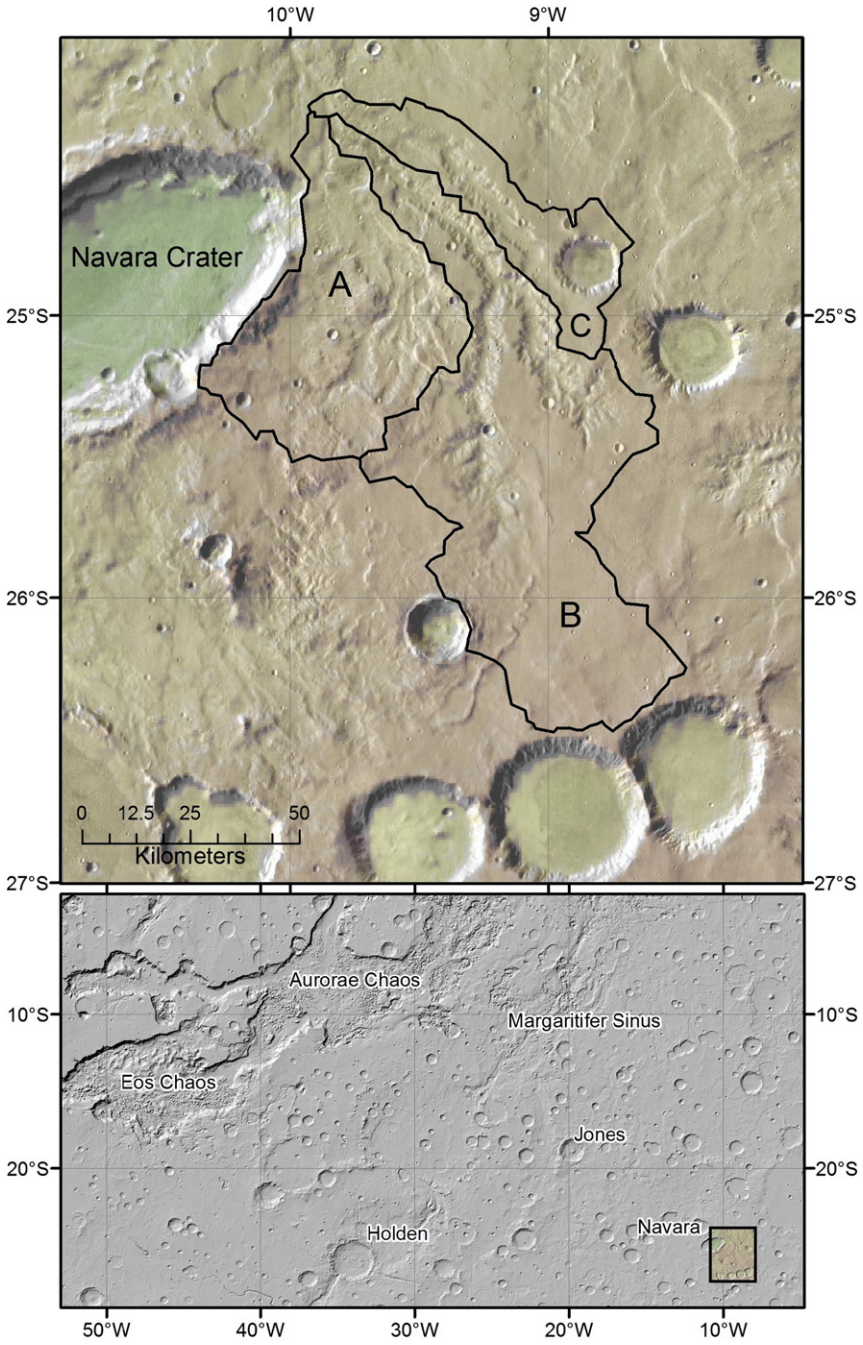

Fig. 1. Regional view of Margaritifer Sinus using MOLA DEM. The Parana Valles study site catchment boundary is highlighted.

The hypsometric integral (HI) is a dimensionless value represented by the area under the hypsometric curve and can be written as:

$$\mathrm{HI} = \frac{\text{Mean elevation} - \text{Minimum Elevation}}{\text{Maximum Elevation} - \text{Minimum Elevation}} \quad (2)$$

High values indicate a large proportion of the catchment exists at higher elevations (Strahler's youthful stage) and vice versa (Strahler's Monadnock stage). As a catchment erodes the hypsometric integral typically decreases. Previously, the hypsometric integral has been used with limited success in the Margaritifer Sinus region of Mars to determine processes behind catchment form (Luo, 2002). However, catchments investigated in this paper are of a higher resolution and smaller area, which improves the ability to interpret the hypsometric integral (Hancock, 2005).

3.3. The cumulative area distribution (CAD)

The CAD is the proportion of the area of the catchment that has a drainage area greater than or equal to a specified drainage area. It was used by Moglen and Bras (1995a,b) to characterise flow aggregation characteristics of channel networks and hillslopes within a catchment. As with the hypsometric curve, the CAD is most useful as a diagram, allowing three regions of differing erosion properties to be identified (Moglen and Bras, 1995b; Perera and Willgoose, 1998) (Fig. 5).

Fig. 2. Shaded images of the study area displaying the catchments and topography (top) and alternate view displaying the entire catchment and surrounds (bottom).

Region I of the curve corresponds to areas of the catchment dominated by diffusive erosion (i.e. upslope areas), Region II depicts the areas dominated by incisive channel flow, and Region III represents areas dominated by large channels connected to the outlet of the catchment. Breaks in the slope of the CAD may be used to more precisely determine where the boundaries of these regions are.

3.4. Width function

The width function of a catchment is a plot of the number of channels at a given distance from the outlet of a catchment (Surkan, 1969). In this study the function has been modified to be incorporated into digital terrain analysis by replacing the channels in the definition with algorithmically generated flow paths created using the flow routing algorithm of SIBERIA (Willgoose, 2005). This avoids some of the issues resulting from differing methods used to calculate drainage paths by using a standard method of channel derivation. It primarily discriminates between different shapes and hydrological responses of catchments (Rinaldo et al., 1995).

3.5. Strahler Order

Strahler Order (or Strahler–Horton Order) is a widely used method to describe tributary hierarchy (Strahler, 1964). Strahler order has been the dominant statistic used on Mars to categorise and describe channel networks since the first Mariner 9 images (McCauley et al., 1972). Willgoose et al. (2003) suggested that its statistical reliability is low. In this study automatic extraction of the channel network from the DEM was used as opposed to visual or qualitative assessment. This allows an unbiased and repeatable assessment of drainage network characteristics.

3.6. Assessment of catchment statistics at the pixel scale

While whole-catchment descriptors are useful for comparisons between catchments, pixel scale analyses are also possible. This overcomes the main weakness of the descriptors, which is their inability to determine intra-catchment differences. In this study, both the area-slope and hypsometric integral were calculated at a pixel scale using methods developed by Cohen et al. (2008).

The DEM was divided into a grid of pixels in which each acted as an outlet node for the upslope pixel in the determination of both D8 flow direction and D_{inf} contributing area. Algorithms where then used to calculate a pixel raster of each variable in the area-slope and hypsometric integral (Eqs. (1) and (2)), before these rasters were combined to derive the α and c values of the area-slope equation and the value of the hypsometric integral.

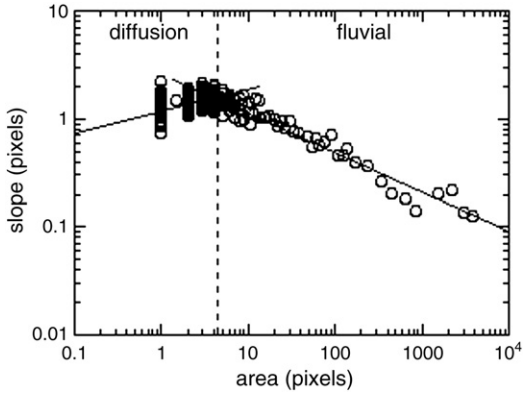

Fig. 3. Physical explanation of the area–slope relationship developed by Willgoose (1994). The plot shows the clear split between diffusive and fluvial regions of a catchment for a terrestrial test catchment.

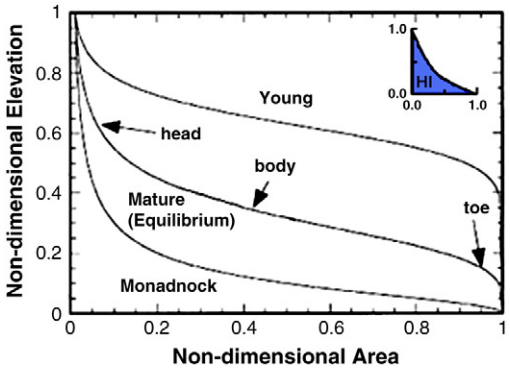

Fig. 4. Time stages (Young, Mature, Mondanock) and curve descriptors (head, body, toe) for the hypsometric curve of Strahler. The inset in the top right corner depicts hypsometric integral as the blue area under the curve (after Strahler, 1964; Ohmori, 1993; Willgoose and Hancock, 1998).

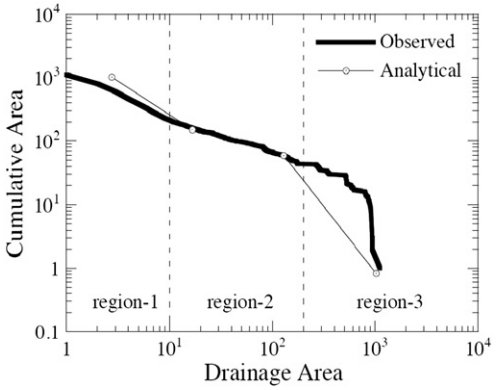

Fig. 5. The cumulative area diagram and regions described (after Perera and Willgoose, 1998).

Results were then averaged over each subcatchment of the Parana study site using zonal statistics based on subcatchment Strahler order. This averaging technique allowed spatial differences in α, c and the hypsometric integral to be recognised while filtering out noise. Cohen et al. (2008) attributed these differences to a variety of spatially varying catchment attributes including the diffusive and fluvial erosive processes that dominate terrestrial catchments. Specifically, differences in (1) α were ascribed to differences in erosivity and soil units, (2) c to differences in morphology, and (3) hypsometric integral values to erosion resistance and landform concavity.

The Getis-Ord G_i^* Hotspot statistic was used as an alternative. This method significantly reduced the pixel noise in the final result. It evaluates association by using a set distance to define a circular 'spot' of values around a particular point. The values are then spatially averaged within the spot, determining the value for the variable at that particular point in the gridded values. This method generates 'hot' (high value) and 'cold' (low value) clusters for analysis that are typically normalised to a range of $-2 \leq \alpha \leq 2$ for comparison. G_i^* analysis has been successfully used by Pérez-Peña et al. (2009) on Earth to examine differences in hypsometric integral between pixels which correlate to tectonic faulting.

3.7. Parameterisation of mineral reflectance

Spectroscopy of the surface of Mars by multiple spacecraft instruments has confirmed that the major rock type on Mars is basalt (Bibring et al., 2006). This lithology is present across ancient Noachian terrains, including the heavily dissected geologic unit where Parana Valles is located. Investigations into the composition of Parana Valles itself by Talib et al. (2007) using the Thermal Emission Spectrometer (TES) identified a mixture of phyllosilicates, feldspars, olivines and pyroxene, which provides geochemical evidence for a basaltic surface that has undergone periods of both fluvial activity and intense degradation when compared to other parts of Mars.

In this investigation, subsequent mineral spectra strips were retrieved from the Compact Reconnaissance Imaging Spectrometer (CRISM) which were mosaicked and overlaid across the area of interest. Spectral summary products derived from key reflectance wavelengths for mineral classes (Pelkey et al., 2007) were then determined. The data, acquired from the Targeted Reduced Data Record (TRDR) described in Murchie et al. (2007) is derived from band 12 (Olivine index—OLINDEX), band 13 (Pyroxene index—LCPINDEX) and 14 (Pyroxene index—HCPINDEX) (filename t0657_mrrsu_25s352_0256_1.img). The data has been atmospherically, photometrically and thermally corrected (Murchie et al., 2007). Fig. 6 demonstrates the relatively spatially homogenous distribution of pyroxene across the study area (LCPINDEX and HCPINDEX) which is likely due to a uniform surface basalt mineralogy. No aqueously altered mineralogy in the detection range of the instrument (e.g. clays, carbonates) was detected.

4. Results

A terrestrial catchment typically has characteristics that are products of factors which control catchment form and function, such as underlying geology and climate (Hancock, 2005). Visual comparison between landscapes is a first step in understanding catchments and the processes that take place within them (Hancock, 2005).

Most of the subcatchments surrounding the Parana Basin are elongated and have few tributaries when compared to terrestrial basins. Flow networks tend to aggregate to channels which are several kilometres wide and range in length from 350 km (main channel) to just tens of kilometres. The catchments of this investigation (Fig. 7) are located within the south-western corner of the Parana Basin (Fig. 1). While the basin is not heavily affected by impact craters compared to other regions, many catchments had significant craters. Catchments were therefore selected which had no or a minimal number of craters which may bias any analysis. The closeness of the subcatchments has been prioritised to reduce possible spatial variations in climate on Mars. It is vital to note that all catchments in the area are likely to have undergone resurfacing from wind, slumping and even impact gardening (Hartmann et al., 2001), which could potentially affect area-elevation analysis as the catchments still had some impact craters present. Subcatchments A, B and C are nested subcatchments within the whole that have been individually investigated in the same manner (Fig. 8).

Catchment relief is similar in A and B (Table 1) and maximum heights are at catchment boundaries adjoining crater rims. The subcatchments are comparable in relief (1 km) to large subcatchments on Earth (Figs. 1, 2), apart from uplifting of elevation due to crater impacts at catchment boundaries and differences in flow paths caused by cratering. Flow paths appear to be controlled by the large impacts at the catchment edges, indicating the channel formation occurred after the Heavy Bombardment era of solar system formation. This therefore reinforces the need for careful catchment selection for reliable analysis based on DEMs. For example, subcatchment B curls around Novara crater (oval), suggesting the impact forced flow around the crater.

A sharp contrast in slope can be seen between the upper and lower regions of the catchments. The upper region contains a smoother, convex surface, before rapidly falling away into dissected channels which cut through hummocky terrain. This contrast is potentially indicative of two distinct types of erosion occurring in the catchment: diffusive processes including soil creep and mass wasting in upper regions and incisive fluvial action in the lower regions.

Uniform surface geology is useful to the study as it can be observed in the distribution of catchment statistics such as the area–slope relationship (Hancock, 2005) so that differences in erosion are more likely to be driven by material particle size and differences relating to erosion intensity rather than differences between geologic units.

4.1. Catchment scale statistical analysis

4.1.1. Area–slope relationship

The area–slope relationships of the subcatchments (Fig. 9) have a much wider scatter in slope around the mean trend than is generally seen on Earth. The slope of the fluvial region (α, Table 1) also indicates that Martian catchments have an area exponent at the lower end of that observed for terrestrial basins (Section 3.1, Eq. (1)). Typical values for α on Earth would be 0.7 in a humid environment (Willgoose et al., 1991; Hancock, 2005) and 0.3–0.5 for semi-arid and arid climate zones. Our Martian catchments have a value of 0.25 or lower. This is indicative of a hyper-arid climate or minimal erosive conditions, which corresponds with current understandings of climate on the planet (Hoke and Hynek, 2009). A diffuse region (see Fig. 3) in the data set is not easily observed most likely due to the coarse resolution of the DEM grid size.

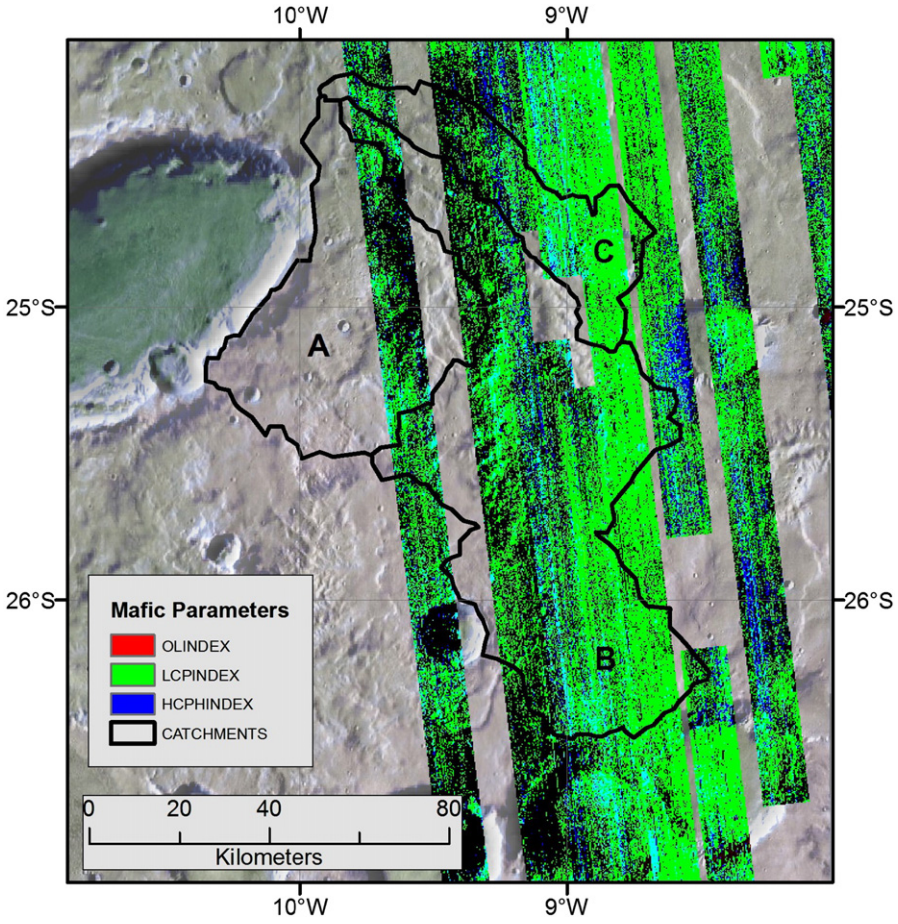

Fig. 6. Map of CRISM mineral spectral summary products overlaid on subcatchment boundaries displaying spectral signatures for olivine (OLINDEX), Low-Mg Pyroxenes (LCPINDEX) and High-Mg Pyroxenes (HCPXINDEX) (Murchie et al., 2007). Colour stretches are those used in a global mineral survey of Mars (Pelkey et al., 2007: Fig. 7).

The parallel area-slope relations for subcatchments A, B and C suggest they have similar area-slope-elevation properties, and are close to the total of these three catchments. Hancock (2005) demonstrated that terrestrial catchments with similar geology display similar area-slope properties and which was first suggested by Willgoose et al. (1991). Stepinski and Stepinski (2005) also demonstrated that close-lying basins have formed under similar climatic properties on Mars. The comparable area-slope relationships of subcatchments A, B and C are indicative that they have undergone the same surface processes and been influenced by similar formation factors.

The large scatter in the slope data for large areas demonstrates the wide variety of gradient changes within each of these catchments which is a possible result of multiple surface processes simultaneously present or differences in the underlying geology creating an erosion regime which is structurally controlled by differences in erodibility between geologic layers (see Willgoose, 1994). We attribute these differences to fracturing below the surface from impact cratering. The high elevation points and hence slope values could also be explained by the inclusion of several greatly uplifted points on crater rims being included in the data set. These points are valid data and must be included in a present-day surface analysis of Mars, however, cases for their removal are presented by Fortezzo and Grant (2004).

4.1.2. Hypsometric curve and integral

The hypsometric results of catchments (Fig. 10) are indicative of mature terrestrial catchments (Strahler, 1964). The head of the curve has a steep negative slope indicating an abrupt drop from the uplifted catchment boundaries. These sharp gradients then give way to unusually linear curve bodies that are not a common feature of terrestrial catchments (Willgoose and Hancock, 1998). Such linearity is potentially due to channel incision into the surface of Mars being far greater in proportion when compared to Earth, generating a hypsometric curve that has an erosion resistant mid-slope area. The value of the hypsometric integral (non-dimensional area under the hypsometric curve) ranged from 0.40 to 0.48 (Table 2), which is within the range for terrestrial values (Strahler, 1964).

4.1.3. Cumulative area distribution (CAD)

The CAD measures the flow aggregation properties of the channel network (e.g. Perera and Willgoose, 1998). The inflection points mark the change in erosion regimes and are barely visible at areas of 4 and 1000 pixels suggesting a transition from diffusive to fluvial erosion not easily observed in the area–slope relationship (Fig. 11a). However, confirmation of erosion regimes can be seen in the slope of the CAD (Fig. 11b).

Region I of the slope of the CAD has a slightly concave up trend (Fig. 11b), which has been observed by Perera and Willgoose (1998) to be indicative of diffusive smoothing processes which operate near catchment boundaries. Region II of the curve obeys the log–log power law observed as being a universal feature of natural terrestrial catchments (La Barbera and Roth, 1994; Perera and Willgoose, 1998). The power curve fits for Region II of the curve agree with terrestrial values that have ranged from 0.42 to 0.56 in simulated and natural catchments (Fig. 12; Perera and Willgoose, 1998).

Region III of the curve rapidly falls, indicating rapid aggregation of areas to large channels when the area approaches total catchment

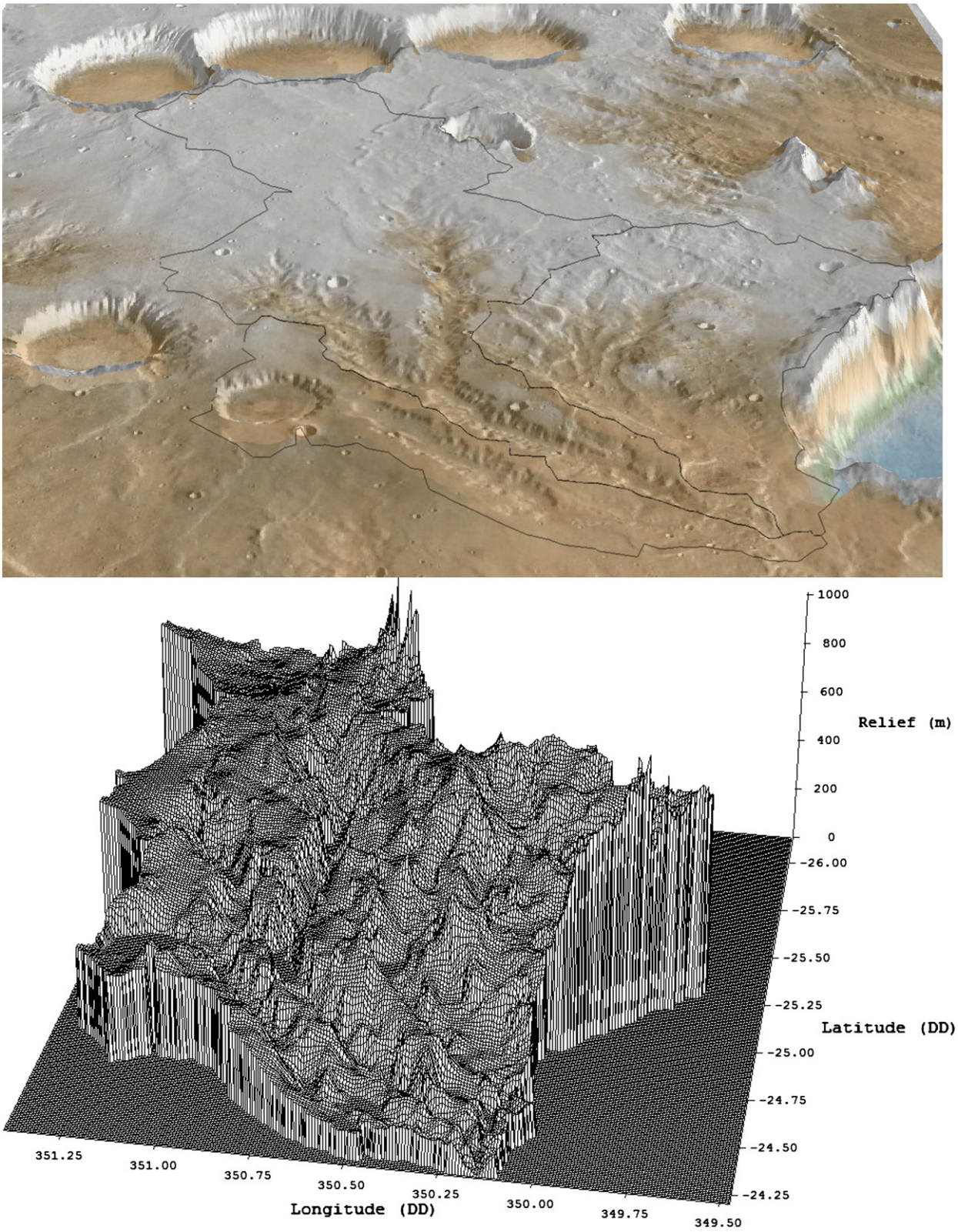

Fig. 7. Three-dimensional representation of the total catchment using MOLA DEM elevation data (top) and DEM of the extracted study area (bottom). Subcatchment A is on the right, B is in the middle and C is at the front. Elevation peaks are due to uplifted crater edges. The viewing point is at the bottom right of Fig. 4. Individual catchments A, B and C are displayed in the following figure.

area. These similar trends are further indication of a diffusive/fluvial/large channel difference in erosion processes in different regions of the catchment.

4.1.4. Width function

The location of peaks and troughs of the normalised width function for each catchment result from differences in catchment shape (Fig. 13).

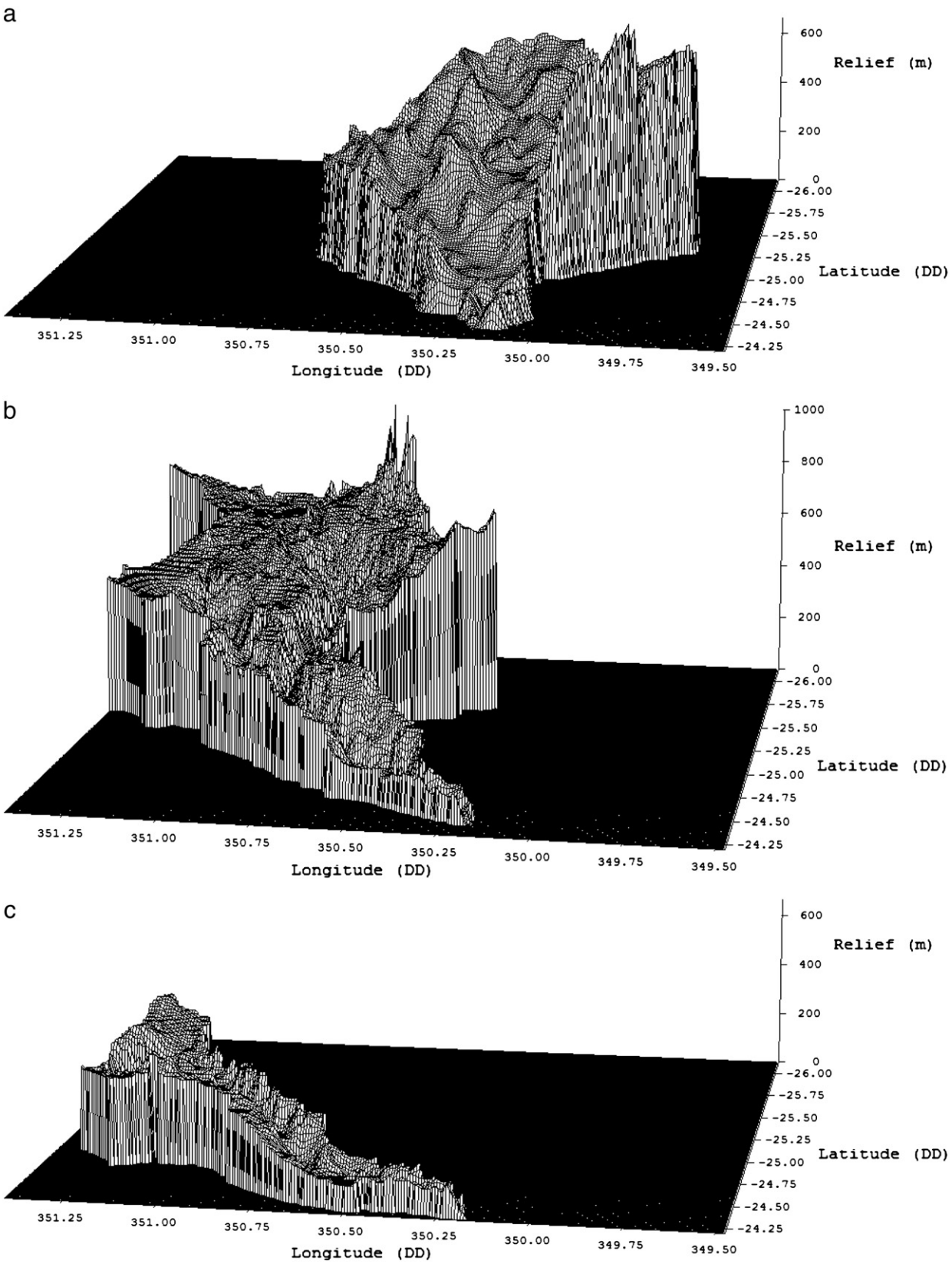

Fig. 8. Three-dimensional representations of subcatchments. In order from top to bottom: A, B and C. See figure above for an image of the combined data set.

A comparison of functions across all basins reveals little clear signal, which has been a clear limitation of the statistic in the past (Hancock et al., 2002; Hancock, 2005). Maximum widths of catchments occur at the 0.5 to 0.75 distance to outlet range, indicating that catchments have an overall teardrop shape which is typical of terrestrial catchments dominated by precipitation and runoff processes.

Table 1
Catchment area and relief statistics of MOLA DEM data for total catchment and the three subcatchments.

Catchment	Area (km^2)	Relief (m)	α Value	HI
Total	6822	1012	0.25	0.40
A	2303	1004	0.25	0.40
B	3411	991	0.25	0.45
C	1108	471	0.30	0.48

4.1.5. Strahler–Horton ratios and convergence values

The main stream of Parana Valles has one of the highest Strahler orders (order = 7) so far measured on Mars. This is much higher than other Strahler orders for networks across the planet, which are typically in the 3rd or 4th order range for Viking data (Cabrol et al., 2001). However the data here has been derived from automatic extraction methods from the DEM.

The bifurcation, length, slope and area ratios of the catchment and internal subcatchments remain well within terrestrial bounds (Table 2). These ratios have been found by Horton (1945), Strahler (1964) and others to be approximately constant on Earth. Similarities in bifurcation, length, slope and area ratios reinforce the idea that Martian catchments have some self similarity, as per terrestrial circumstances. Our bifurcation ratio (R_b) of 4.8 is high compared to flat terrain on Earth ($R_b = 2$) and lies in the range of mountainous catchments (Horton, 1945) and is consistent with scaling models for network form (Tokunaga, 1978). It is much higher than the average Cabrol et al. (2001) determined for 2208 valley networks using Viking Orbiter data sets ($R_b = 2$). Our higher R_b is likely due to the higher resolution of the MOLA DEM identifying more lateral tributaries and network branching than that obtained from the Viking data. It should be noted that the Strahler order data here have been derived using automatic extraction from the DEM which removes the need for qualitative assessment from images. Therefore differences in Strahler order and derived statistics will result in differences between our quantitative data and that of the qualitative data derived from photography. The method removes any subjectivity and provides a robust and repeatable method based on the DEM.

4.2. Pixel scale statistical analysis

4.2.1. Area–slope exponent α

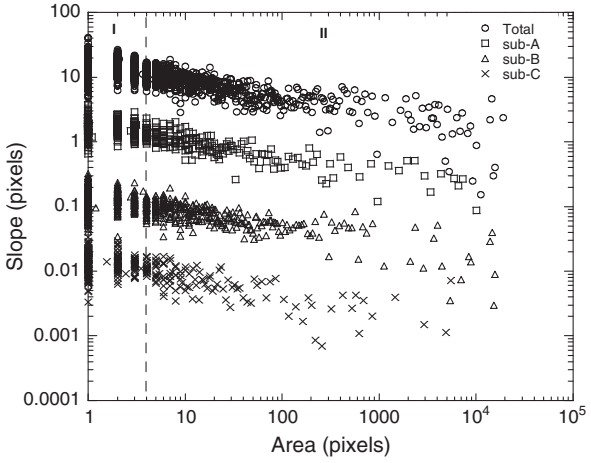

Fig. 9. Averaged area–slope relationship for the total catchment and subcatchments A, B and C. For ease of viewing results the slopes of the subcatchments A, B and C have been divided by 10, 100 and 1000 respectively.

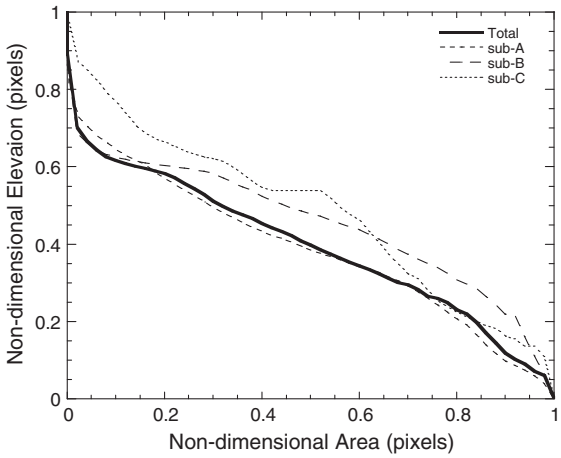

Fig. 10. Hypsometric curve results comparing the total catchment against subcatchments A, B and C. Taking aging stages from Strahler (1964), all catchments are of a mature composition.

This section uses the methodology of Cohen et al. (2008). The spatial distribution of the area exponent of the area–slope relationship (α) is important to investigate as it can be used to determine regions of diffusive (smoothing) and fluvial (incisive) processes in a catchment. Willgoose et al. (1991) proposed a process-based explanation for the area–slope relationship and (1) can be represented by two equations for diffuse and fluvial erosion respectively,

$$S = \left(\frac{U}{D}\right)A_s^{\alpha} \quad \text{and} \quad \left(\frac{U}{\beta_1\beta_3}\right)^{\frac{1}{n_1}} A^{\frac{1-m_1m_3}{n_1}} \propto A^{\alpha} \tag{3}$$

where A is the area draining through a defined point in the catchment, α is the scaling exponent, S is the slope of the point, U is the tectonic uplift of the catchment and m_1, n_1 , β_3 and m_3 are constant parameters.

This equation can be solved spatially for both α and the constant, *c*, the coefficient in Eq. (2) from elevation and slope data at every pixel in a DEM. A high α value is more likely to be a diffusive dominant region in the catchment that contains erosion resistant material. A negative α represents incisive fluvial erosion, where slope decreases as contributing area increases. A pixel by pixel plot of α and *c* is very noisy.

To filter the noise the α values for every pixel in each of these subcatchments were then averaged using zonal statistics to determine the mean α value for each subcatchment. The resultant raster data sets describe the subcatchment averaged spatial distribution of α within the total catchment investigated (Fig. 14).

Table 2
Summary of all statistics for the total catchment and subcatchments A–C. Terrestrial range derived from Horton (1945) and Ibbitt et al. (1999).

	Total catchment	A	B	C	Terrestrial range
Strahler Order	7	6	7	6	1–12
Bifurcation ratio	4.87	4.85	4.87	4.80	2.0–8.0
Length ratio	1.5	1.43	1.56	1.46	0.5–3
Slope ratio	1.55	1.69	1.50	1.46	0.5–2.0
Area ratio	5.16	5.10	5.24	5.11	3.5–8.0
Flint θ	0.30	0.33	0.29	0.29	0.2–0.7
α Value	0.25	0.25	0.25	0.30	0.2–0.7
Convergence	1.48	1.47	1.48	1.56	1–3
Probability of branching	0.32	0.31	0.32	0.35	0–1

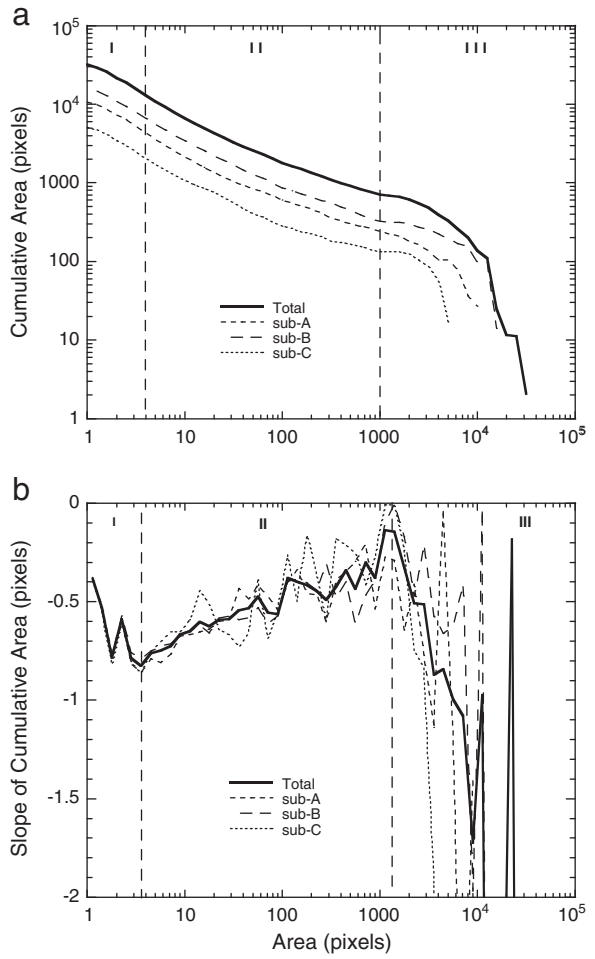

Fig. 11. (a) CAD distribution for the total catchment and subcatchments A, B and C and (b) slope of the CAD Distribution for the above. Erosion regime divisions are marked by dotted lines.

The 3rd order raster is relatively noisy, while the 4th order raster shows some general trends over the catchment. The 5th order raster develops the clearest results. Higher averaging (e.g. 6th or 7th order) simplifies results into too few subcatchments to resolve spatial trends.

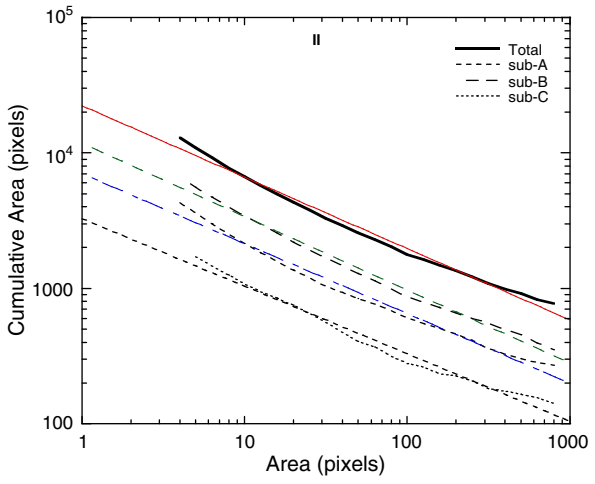

Fig. 12. A close-up of Region II with power curve fits, demonstrating the log–log power relationship of area and cumulative area (negative exponent of the curve).

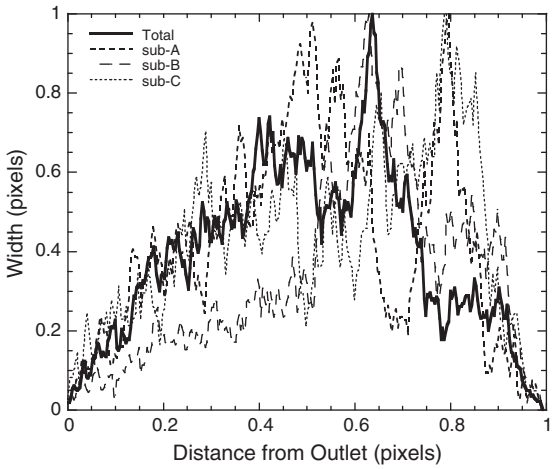

Fig. 13. Width function for the total catchment and subcatchments A–C with both axis normalised.

The map of α values has extreme low values in the northwest and southeast corners of the catchment (the regions of highest elevation). In previous work, on Earth, Cohen et al. (2008), interpreted these high value subcatchments as clay soils within their study area on Earth, which were relatively resistant to erosion compared with the remainder of total catchment. In this study these high α values correspond to the lower highly channelised section of the catchment.

However, the Gi* hot-spot analysis (Fig. 14d) provides a much clearer indication of how the high values in the lower catchment, though dominant, are separated by low values in each trunk channel. It is likely that these areas are much more vulnerable to erosion (having a much higher contributing area), but were masked by the subcatchment averaging method.

As the catchments are suggestive of being geologically homogenous from mineral spectral survey and subcatchment mapping (Section 3.6), it is likely that differences in α values are caused by dissimilarities in surface processes, rather than geologic units. This contrasts with the terrestrial study of Cohen et al. (2008), and Hancock (2005) that linked differences in geology and erosion resistance to differences in the area–slope relationship.

4.2.2. Area-slope coefficient c

The constant of the area–slope relationship also provides information about the erosive processes occurring in a catchment. Higher values of *c* represent areas of fluvial erosion while low values of *c* indicate dominance of diffusive erosion.

Values for *c* are quite variable across the 3rd and 4th order scale. However, when observing the Gi* hot-spot analysis it becomes clear that many of the high values in the channelised, fluvial areas of the catchment are lost in the subcatchment averaging (Fig. 15). The fork of the two main channels in subcatchment C is clearly visible as a high *c* region which should be dominated by incisive processes.

4.2.3. Hypsometric integral (HI)

Willgoose and Hancock (1998) related the hypsometric curve and integral for geologically uniform and equilibrium catchments to the concavity of the landscape rather than the traditional interpretation of surface maturity (Strahler, 1964). They found a general catchment scale relationship between convex curvature in the hypsometric curve, a high hypsometric integral and a diffusive dominated erosion process, while a concave curvature was related to a lower hypsometric integral and a more incisive fluvial process.

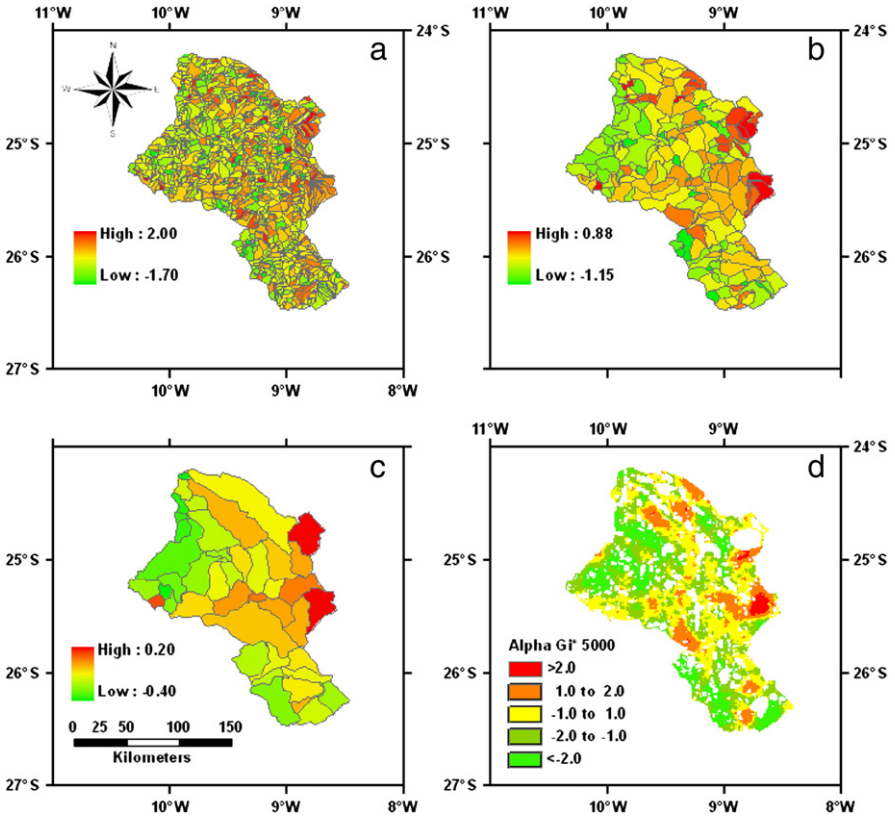

Fig. 14. Spatial distribution of parameter α for (a) third, (b) fourth and (c) fifth order subcatchment averaging and (d) Gi_i^* hot-spot analysis of α values. The value of each subcatchment is the average of all pixels within the subcatchment, except in (d), where values represent relative clusters of high and low values. Pixels of no value in (d) were excluded because they fell outside $-2 \leq \alpha \leq 2$.

However, this hypothesis is not relatable to the distribution of values over the study site. Instead high value pixels occur in the lower regions of the catchment (Fig. 16). Hence, it may be likely that the explicit spatial solution to the hypsometric integral is not a valid indicator of the diffusive/fluvial division in erosion regimes. These high value pixels potentially mask nearby lower value pixels which are not resolvable using Gi* hot-spot analysis. Pérez-Peña et al. (2009), using a similar pixel-by-pixel method to solve the hypsometric integral spatially, determined that, in dissected landscapes, high values were indicative of dissected pixels with a high gradient and low value pixels on smooth surfaces. This hypothesis seems more consistent with the results.

When an erosion-resistant surface unit exists (e.g. Barnhart et al., 2009), this distribution of HI values is compatible with the idea that erosion resistant materials and diffusive processes are dominant across the less dissected regions of subcatchments A and C, while fluvial processes are dominant in channelised regions. Walcott and Summerfield (2007) and Cohen et al. (2008) both found that subcatchment averaging of the hypsometric integral indicated similar trends between subcatchment hypsometric integral and erosion resistance.

These results also correspond with the manually extracted catchment trend indicated by the hypsometric curve (Fig. 10). The middle section is unusually linear and different from a terrestrial hypsometric curve which has a clear inflection marking the diffusive/fluvial erosion regime change.

5. Discussion

The catchments investigated in this study have area, slope, elevation, width and networking characteristics that correspond to the known range for catchments on Earth. This analysis supports previous geomorphic conclusions about Mars, but remains the first to examine a suite of geomorphic and hydrologic properties that allow cross-verification and comparison of data. The information provided in the assessment of a Martian catchment's form corresponds with what we know about the distribution of these statistics on Earth (Willgoose, 1994; Perera and Willgoose, 1998; Cohen et al., 2008). Using these terrestrial explanations allows us to explore what role different surface properties and processes have on landscape morphology. Further, the methods and geomorphic tools described here are employable at other sites and are likely to be useful elsewhere on Mars.

In the smoother hillslope area of the catchment, below the crater uplifted boundaries, fluvial processes are likely to be dominant, as demonstrated by the log–log linearity of the area–slope relationship (Fig. 8) and the distribution of the α and HI (Figs. 13, 15). In terrestrial studies, large scatter in the slopes in the area–slope relationship has previously been attributed to geological heterogeneity across the landscape causing differences in erosion resistance and hence the landscape surface (Hancock, 2005). However, here it is suggested from the remote sensing of the relatively homogeneous basalt unit (Fig. 6) that the surface is likely to be one geologic unit and hence differences in erosion resistance are more likely to be attributable to physical characteristics of the material.

Remnant patches of erosion resistant material may occur which match the distribution of α in Fig. 14, which is a terrestrial indicator of erosion resistance (Cohen et al., 2008). The distributions also indicate that the regions between such patches are likely to be dominated by incisive, channelised erosion.

The hypsometric curve (Fig. 10) also matches those seen in fluvial catchments on Earth, despite the uplifted crater edges. Similarities to simulations by Hancock (unpublished) that used an experimental catchment with an erosion resistant upper region indicate that the

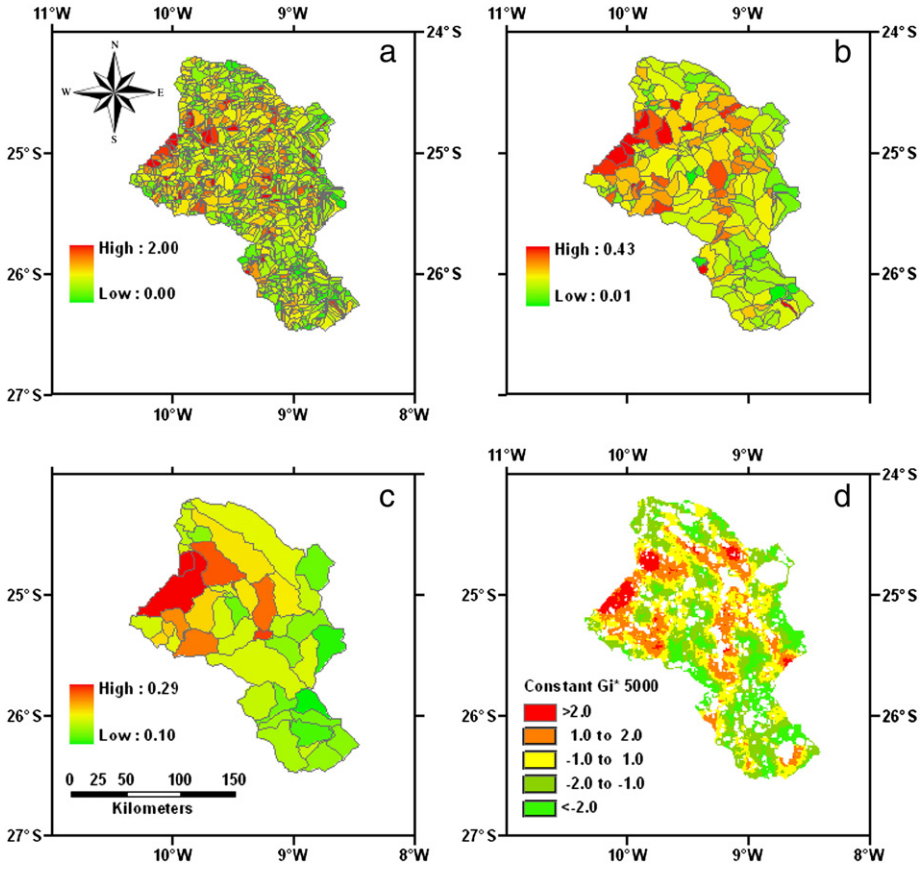

Fig. 15. Spatial distribution of parameter *c* for (a) third, (b) fourth and (c) fifth order subcatchment averaging and (d) Gi_i^* hot-spot analysis of *c* values.

crater uplifted edges of the catchment are likely to be less eroded due to a reduced area for rainfall to impact on. The hypsometric integral (area under the hypsometric curve) is relatively low when compared to previous values across the Margaritifer Sinus (Fortezzo and Grant, 2004) and concurs with the values used by Luo (2002) to distinguish fluvial-like catchments from sapping-like.

The fluvial section of the CAD (Fig. 12) has a slope ($\Phi = -0.5$) typical of natural catchments on Earth formed by precipitation and surface overland flow. This may be the result of self-organisation within catchments. The similarity of the Martian CADs to Earth is indicative that channels form at a similar threshold area which is proportionate to channels formed by rainfall and runoff on Earth. Whether this is a universal feature of all landscapes should be subject to further research on Earth, Mars and other planetary bodies.

The area-aggregation properties are consistent with the findings of Fasset and Head (2008). They correlated the area of depressions on Mars thought to be open-basin lakes with the size of potential watersheds that could have generated them.

In terms of similarity, all statistics demonstrate a range of plots and values that lie within the known bounds of terrestrial fluvial catchments and demonstrate that the catchment landscape has a shape and form similar to catchments on Earth carved by water (Table 2).

6. Conclusion

Examination of terrestrial catchment statistics applied to the study catchments in the Parana Valles region suggests that these basins have similar geomorphic and hydrologic properties to catchments formed by precipitation and runoff on Earth. Intra-catchment statistics determined by the utilisation of a novel method for spatial analysis of the area–slope relationship and hypsometric integral on a pixel-by-pixel basis significantly enhanced results and uncovered differences in erodibility across the catchments which were not reflected in analysis of remotely sensed mineral detections from CRISM spectral summary products. While only used for several relative small catchments with few impact craters, the methods used here are applicable to other areas on Mars where fluvial processes are believed to have shaped the surface.

Understanding the Martian surface through geomorphologic and hydrologic investigations of the landscape may be the only method we can use to address whether water flow in substantial quantities has occurred on Mars in the past, given the change of climate conditions believed to have occurred at the end of the Noachian period (3.7 Ga) (Solomon et al., 2005; Bibring et al., 2006). The findings here are indicative of a hyper-arid climate or minimal erosive conditions, which corresponds with current understandings of climate on the planet. However, it is recognised that the erosion processes that formed the catchments examined here may have been subjected to periods of enhanced rainfall. One postulated process for enhanced rainfall periods water injected into the atmosphere from impacts producing precipitation at unknown rates and intensities. The authors intend to continue the explore methods for further understandings into fluvial processes on Mars.

Acknowledgements

BN received support from a Faculty of Science and IT Summer Scholarship as well as a School of Engineering Honours Scholarship. GRW was supported by an Australian Research Council Professorial Fellowship.

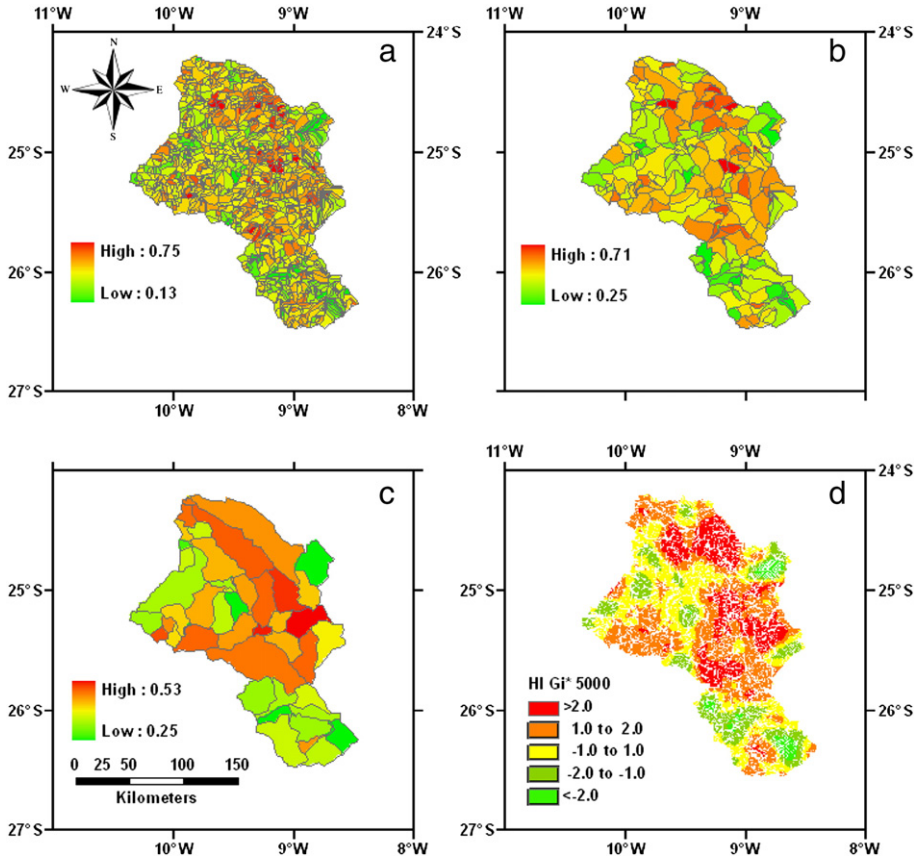

Fig. 16. Spatial distribution of the hypsometric integral for (a) third, (b) fourth and (c) fifth order subcatchment averaging and (d) Gi_i^* hot-spot analysis of hypsometric integral values. Pixels with no data are a result of pixels having a null hypsometric integral (maximum elevation = minimum elevation).

Dr. Ernst Hauber and an anonymous reviewer are thanked for their thoughtful and constructive comments.

References

Ansan, V., Mangold, N., 2006. New observations of Warrego Valles, Mars: evidence for precipitation and surface runoff. Planetary and Space Science 54, 219–242.
Barnhart, C., Howard, A., Moore, J., 2009. Long-term precipitation and late-stage valley network formation: landform simulations of Parana Basin, Mars. Journal of Geophysical Research 114, E01003–E01024.
Bibring, J., Langevin, Y., Mustard, J.F., Poulet, F., Arvidson, R., Gendrin, A., Gondet, B., Mangold, N., Pinet, P., Forget, F., Berthé, M., Gomez, C., Jouglet, D., Soufflot, J., Vincendon, M., Combes, M., Drossart, P., Encrenaz, T., Fouchet, T., Merchiorri, R., Belluci, G., Altieri, F., Formisano, V., Capaccioni, F., Cerroni, P., Coradini, A., Fonti, S., Korablev, O., Kottsov, V., Ignatiev, N., Moroz, V., Titov, D., Zasova, L., Loiseau, D., Douté, S., Schmitt, B., Sotin, C., Hauber, E., Hoffmann, H., Jaumann, R., Keller, U., Arvidson, R., Duxbury, T., Neukum, G., 2006. Global mineralogical and aqueous Mars history derived from OMEGA/Mars Express data. Science 312, 400–404.
Cabrol, N., Wynn-Williams, D., Crawford, D., Grin, E., 2001. Recent aqueous environments in Martian impact craters: an astrobiological perspective. Icarus 154, 98–112.
Carr, M., 1981. The Surface of Mars. Yale University Press, New Haven. 229 pp.
Carr, M., 1996. Water on Mars. Oxford University Press, New York. 229 pp.
Cohen, S., Willgoose, G.R., Hancock, G.R., 2008. A methodology for calculating the spatial distribution of the area–slope equation and the hypsometric integral within a catchment. Journal of Geophysical Research 113, F03027.
Craddock, R., Howard, A., 2002. The case for rainfall on a warm, wet early Mars. Journal of Geophyscial Research 107, 1–35.
Fasset, C.I., Head, J.W., 2008. Open-basin lakes on Mars: implications of valley networks lakes for the nature of Noachian hydrology. 39th Lunar and Planetary Science Conference, (Lunar and Planetary Science XXXIX), held March 10–14, 2008 in League City, Texas. LPI Contribution No. 1391., p. 1139.
Flint, J.J., 1974. Stream gradient as a function of order, magnitude and discharge. Water Resources Research 6, 969–973.
Fortezzo, C.M., Grant, J.A., 2004. Hypsometric analyses of Martian basins: comparison to terrestrial, lunar and Venusian hypsometry. 35th Lunar and Planetary Science Conference, p. 1647.
Grant, J.A., 1997. Geologic mapping and drainage basin analysis in Margaritifer Sinus, Mars. Lunar and Planetary Science 1672 (XXVIII).
Grant, J.A., 1998. Geologic mapping and drainage basin morphometry in Margaritifer Sinus, Mars. Lunar and Planetary Science 1285 XXIX.
Grant, J.A., 2000. Valley formation in Margaritifer Sinus, Mars, by precipitation-recharged groundwater sapping. Geology 28, 223–226.
Grant, J.A., Parker, T.J., 2002. Drainage evolution in the Margaritifer Sinus region, Mars. Journal of Geophysical Research 107, 1–19.
Hancock, G.R., 2005. The use of digital elevation models in the identification and characterization of catchments over different grid. Hydrological Processes 19, 1727–1749.
Hancock, G.R., unpublished. Experimental testing of the SIBERIA landscape evolution model. PhD. Thesis, University of Newcastle, Newcastle, New South Wales, Australia.
Hancock, G.R., Willgoose, G.R., Evans, K.G., 2002. Testing of the SIBERIA landscape evolution model using the Tin Camp Creek, Northern Territory, Australia, field catchment. Earth Surface Processes and Landforms 27, 125–143.
Hartmann, W.K., Anguita, J., De La Casa, M.A., Berman, D.C., Ryan, E.V., 2001. Martian cratering 7: the role of impact gardening. Icarus 149, 37–53.
Hoke, M.T., Hynek, B.M., 2009. Roaming zones of precipitation on Mars as recorded in valley networks. Journal of Geophysical Research 114, E08002.
Horton, R.E., 1945. Erosional development of streams and their drainage basins: hydrophysical approach to quantitative geomorphology. Geological Society of America Bulletin 56, 275–370.
Howard, A.D., 2007. Simulating the development of Martian highland landscapes through the interaction of impact cratering, fluvial erosion and variable hydrologic forcing. Geomorphology 91, 332–363.
Hynek, B.M., Phillips, R.J., 2001. Evidence for extensive denudation of the Martian highlands. Geology 29 (5), 407–410.
Hynek, B.M., Phillips, R.J., 2003. New data reveal mature, integrated drainage systems on Mars indicative of past precipitation. Geology 31, 757–760.
Ibbitt, R.P., Willgoose, G.R., Duncan, M.J., 1999. Channel network simulation models compared with data from the Ashley River, New Zealand. Water Resources Research 35, 3875–3890.
La Barbera, P., Roth, G., 1994. Invariance and scaling properties in the distributions of contributing area and energy in drainage basis. Hydrological Processes 8, 125–135.
Langbein, W.B., 1947. Topographic characteristics of drainage basins. US Geological Society Water Supply Paper 968-C. United States Geological Society, Washington D.C., pp. 125–157.
Luo, W., 2002. Hypsometric analysis of Margaritifer Sinus and origin of valley networks. Journal of Geophysical Research 107, 5071. http://dx.doi.org/10.1029/2001JE001500.

McCauley, J., Carr, M., Cutts, J., Hartmann, W., Masursky, H., Milton, D., Sharp, R., Wilhelms, D., 1972. Preliminary Mariner 9 report on the geology of Mars. Science 17, 289–327.
Moglen, G.E., Bras, R.L., 1995a. The effect of spatial heterogeneities on geomorphic expression in a model of basin evolution. Water Resources Research 31, 2613–2623.
Moglen, G.E., Bras, R.L., 1995b. The importance of spatially heterogeneous erosivity and the cumulative area distribution within a basin evolution model. Geomorphology 12, 173–185.
Murchie, S., Guinness, E., Slavney, S., 2007. Mars Reconnaissance Orbiter CRISM DATA PRODUCT SOFTWARE INTERFACE SPECIFICATION Version 1.3.5. http://geo.pds.nasa.gov/missions/mro/crism.htm2007(accessed 15 February 2012).
Ohmori, H., 1993. Changes in the hypsometric curve through mountain building resulting from concurrent tectonics and denudation. Geomorphology 8, 263–277.
Pelkey, S.M., Mustard, J.F., Murchie, S., Clancy, R.T., Wolff, M., Smith, M., Milliken, R., Bibring, J., Gendrin, A., Poulet, F., Langevin, Y., Gondet, B., 2007. CRISM multispectral summary products: parametrizing mineral diversity on Mars from reflectance. Journal of Geophysical Research 112, E08S14. http://dx.doi.org/10.1029/2006JE002831.
Perera, H., Willgoose, G., 1998. A physical explanation of the cumulative area distribution curve. Water Resources Research 34, 1335–1343.
Pérez-Peña, J.V., Azañón, J.M., Booth Rea, G., Azor, A., Delgado, J., 2009. Differentiating geology and tectonics using a spatial autocorrelation technique for the hypsometric integral. Journal of Geophysical Research 114, F02018.
Pieri, D., 1980. Martian valleys: morphology, distribution, age, and origin. Science 210, 895–897.
Rinaldo, A., Vogel, G.K., Rigon, R., Rodriguez-Iturbe, I., 1995. Can one gauge the shape of a basin? Water Resources Research 31 (4), 1119–1127.
Scott, D., Tanaka, K., 1986. Geologic map of the western equatorial region of Mars. United States Geological Survey. 1:15,000,000.
Solomon, S.C., Aharonson, O., Aurnou, J.M., Banerdt, W.B., Carr, M.H., Dombard, A.J., Frey, H.V., Golombek, M.P., Hauck II, S.A., Head III, J.W., Jakosky, B.M., Johnson, C.L., McGovern, P.J., Neumann, G.A., Phillips, R.J., Smith, D.E., Zuber, M.T., 2005. New perspectives on ancient Mars. Science 307, 1214–1220.
Squyres, S., Kasting, J., 1994. Early Mars: how warm and how wet? Science 265 (5173), 744–749. http://dx.doi.org/10.1126/science.265.5173.744 (5 August 1994).
Stepinski, T.F., Stepinski, A.P., 2005. Morphology of drainage basins as an indicator of climate on early Mars. Journal of Geophysical Research 110, E12S12. http://dx.doi.org/10.1029/2005JE002448.
Strahler, A.N., 1964. Quantitative geomorphology of drainage basins and channel networks. In: Chow, V.T. (Ed.), Handbook of Applied Hydrology. McGraw-Hill, New York, p. 1467. p. 4-39–4-76.
Surkan, A.J., 1969. Synthetic hydrographs: effects of network geometry. Water Resources Research 5, 112–128.
Talib, S., Dalton, J.B., Moore, J.M., 2007. Search for aqueous minerals in Parana Valles, Mars. Bulletin of the American Astronomical Society 39, 434.
Tarboton, D.G., Bras, R.L., Rodriguez-Iturbe, I., 1989. The analysis of river basins and channel networks using digital terrain data, TR 326. Department of Civil and Environmental Engineering, Massachusetts Institute of Technology (MIT), Boston.
Tokunaga, E., 1978. Consideration of the composition of drainage networks and their evolution. Tokyo Metropolitan University Geographical Report 13.
Vogt, J.V., Colombo, R., Bertolo, F., 2003. Deriving drainage networks and catchment boundaries: a new methodology combining digital elevation data and environmental characteristics. Geomorphology 53, 281–298.
Walcott, R.C., Summerfield, M., 2007. Scale dependence of hypsometric integrals: an analysis of southeast African basins. Geomorphology 96, 174–186.
Willgoose, G.R., 1994. A physical explanation for an observed area–slope–elevation relationship for catchments with declining relief. Water Resources Research 30, 151–159.
Willgoose, G.R., 2005. Mathematical modeling of whole-landscape evolution. Annual Review of Earth and Planetary Sciences 33, 443–459.
Willgoose, G.R., Hancock, G.R., 1998. Revisiting the hypsometric curve as an indicator of catchment form and process in transport-limited catchment. Earth Surface Processes and Landforms 23, 611–623.
Willgoose, G.R., Bras, R.L., Rodriguez-Iturbe, I., 1991. A physical explanation of an observed link area–slope relationship. Water Resources Research 27, 1697–1702.
Willgoose, G.R., Hancock, G.R., Kuczera, G., 2003. A framework for the quantitative testing of landform evolution models. In: Wilcock, P.R., Iverson, R.M. (Eds.), Predictions in Geomorphology. American Geophysical Union, Washington DC, pp. 195–216.